adaptive neighborhood [8]. For the proposed algorithm, it may be possible to set the parameter $\eta[m, n]$ in a more elaborative way such that the amplitude of the relative entropy is fully exploited.

APPENDIX

In this Appendix, we present the derivation of (13) and (17). To derive (13), we assume that $\bar{\mathbf{x}}_1 > \bar{\mathbf{x}}_2 > \cdots > \bar{\mathbf{x}}_{N-1} > 0$ and $\bar{\mathbf{x}}_k > \bar{\mathbf{x}}_0 > \bar{\mathbf{x}}_{k+1}$ $(N-2 > k \geq 1)$. Using (6) and (9), we have

$$\begin{aligned}\bar{\mathbf{C}} &= \frac{1}{N}\left(\sum_{n=0}^{k}(\bar{\mathbf{x}}_n - \bar{\mathbf{x}}_0) + \sum_{n=k+1}^{N-1}(\bar{\mathbf{x}}_0 - \bar{\mathbf{x}}_n)\right) \\ &= -\frac{M}{N}\log\left(\prod_{n=0}^{k}\frac{x_n}{x_0}\prod_{n=k+1}^{N-1}\frac{x_0}{x_n}\right). \end{aligned} \tag{25}$$

The grayscale-based representation of $\bar{\mathbf{C}}$, denoted by C, is given by $\bar{\mathbf{C}} = -M\log(C/M)$. From the above results, we can write

$$\begin{aligned}\frac{\bar{\mathbf{C}}}{M} &= -\frac{1}{N}\log\left(\prod_{n=0}^{k}\frac{x_n}{x_0}\prod_{n=k+1}^{N-1}\frac{x_0}{x_n}\right) \\ &= \log\left(\frac{C}{M}\right). \end{aligned} \tag{26}$$

Therefore, we have

$$\frac{C}{M} = \left(\prod_{n=0}^{k}\frac{x_n}{x_0}\prod_{n=k+1}^{N-1}\frac{x_0}{x_n}\right)^{1/N}. \tag{27}$$

Equation (13) can now be easily derived from (27).

We now derive (17). From (14), we can write

$$\log\hat{C}_g = \log\frac{x_0}{G} = \log\frac{x}{A} + \log\frac{A}{G}. \tag{28}$$

We note that $A = S/N$ $(S = \sum_{n=0}^{N-1} x_n)$ and $\log(A/G) = D(Q\|P)$. Equation (17) can be easily derived from (28) by making the substitutions and using the definition $I_P(x_0) = -\log(x_0/S)$.

REFERENCES

[1] M. Jourlin and J.-C. Pinoli, "A model for logarithmic image processing," *J. Microsc.*, vol. 149, pp. 21–35, 1988.

[2] G. Deng, L. W. Cahill, and G. R. Tobin, "The study of logarithmic image processing model and its application to image enhancement," *IEEE Trans. Image Process.*, vol. 4, no. 4, pp. 506–512, Apr. 1995.

[3] M. Jourlin and J.-C. Pinoli, "Image dynamic range enhancement and stabilization in the context of the logarithmic image processing model," *Signal Process.*, vol. 41, pp. 225–237, 1995.

[4] M. Jourlin, J.-C. Pinoli, and R. Zeboudj, "Contrast definition and contour detection for logarithmic images," *J. Microsc.*, vol. 156, pt. 1, pp. 33–40, 1989.

[5] G. Deng and J.-C. Pinoli, "Differentiation-based edge detection using the logarithmic image processing model," *J. Math. Imag. Vis.*, vol. 8, no. 2, pp. 161–180, 1998.

[6] P. Gremillet, M. Jourlin, and J.-C. Pinoli, "LIP-model-based three-dimensional reconstruction and visualization of HIV infected entire cells," *J. Microsc.*, vol. 174, pp. 31–38, 1994.

[7] G. Courbebaisse, F. Trunde, and M. Jourlin, "Wavelet transform and lip model," *Image Anal. Stereol.*, vol. 21, pp. 121–125, 2002.

[8] J.-C. Pinoli and J. Debayle, "Logarithmic adaptive neighborhood image processing (lanip): Introduction, connections to human brightness perception, and application issues," *EURASIP J. Adv. Signal Process.*, vol. 2007, 2007, 22 pp. Article ID 36 105 doi:10.1155/2007/36105.

[9] J. M. Palomares, J. Gonzalez, E. R. Vidal, and A. Prieto, "General logarithmic image processing convolution," *IEEE Trans. Image Process.*, vol. 15, no. 11, pp. 3602–3608, Nov. 2006.

[10] J.-C. Pinoli, "A general comparative study of the multiplicative homomorphic, log-ratio and logarithmic image processing approaches," *Signal Process.*, vol. 58, no. 1, pp. 11–45, 1997.

[11] I. H. Woodhouse, "The ratio of the arithmetic to the geometric mean: A cross entropy interpretation," *IEEE Trans. Geosci. Remote Sens.*, vol. 39, no. 1, pp. 188–189, Jan. 2001.

[12] S. F. Gull and J. Skilling, "Maximum entropy method in image processing," *IEE Proc. Part F-Commun.*, vol. 131, no. 6, pp. 646–659, 1984.

[13] D. J. C. MacKay, *Information Theory, Inference and Learning Algorithms*. Cambridge, U.K.: Cambridge Univ. Press, 2003.

[14] M. Perisastry and V. N. Murty, "Bounds for the ratio of the arithmetic mean to the geometric mean," *The Two-Year College Math. J.*, vol. 13, pp. 160–161, 1982.

[15] R. E. Glaser, "The ratio of the geometric mean to the arithmetic mean for a random sample from a gamma distribution," *J. Amer. Statist. Assoc.*, vol. 71, pp. 480–487, 1976.

Phase-Adaptive Superresolution of Mammographic Images Using Complex Wavelets

Alexander Wong, *Member, IEEE*, and
Jacob Scharcanski, *Senior Member, IEEE*

***Abstract*—This correspondence describes a new superresolution approach for enhancing the resolution of mammographic images using complex wavelet frequency information. This method allows regions of interest of a mammographic image to be viewed in enhanced resolution while reducing the patient exposure to radiation. The proposed method exploits the structural characteristics of breast tissues being imaged and produces higher resolution mammographic images with sufficient visual fidelity that fine image details can be discriminated more easily. In our approach, the superresolution problem is formulated as a constrained optimization problem using a third-order Markov prior model and adapts the priors based on the phase variations of the low-resolution mammographic images. Experimental results indicate the proposed method is more effective at preserving the visual information when compared with existing resolution enhancement methods.**

***Index Terms*—Adaptive, mammography, phase, superresolution.**

I. INTRODUCTION

Breast cancer is one of the most common types of cancer and is one of the leading causes of cancer death worldwide. To reduce the risk of death due to breast cancer, it is important to detect and treat breast cancer in its early stages. One of the most effective methods for detecting breast cancer is through the use of mammography, where a

Manuscript received September 10, 2008; revised November 28, 2008. First published March 16, 2009; current version published April 10, 2009. This work was supported in part by the Natural Sciences and Engineering Research Council of Canada. The associate editor coordinating the review of this manuscript and approving it for publication was Dr. Pier Luigi Dragotti.

A. Wong is with the Systems Design Engineering, University of Waterloo, Waterloo, N2L 3G1 Canada (e-mail: a28wong@engmail.uwaterloo.ca).

J. Scharcanski is with the Systems Design Engineering, University of Waterloo, Waterloo, N2L 3G1 Canada, and also with the Instituto de Informatica, Universidade Federal do Rio Grande do Sul, Caixa Postal 15064, 91501-970, Porto Alegre, RS, Brasil (e-mail: jacobs@inf.ufrgs.br).

Digital Object Identifier 10.1109/TIP.2009.2013077

breast radiograph is acquired and analyzed for possible signs of abnormality, such as the presence of masses and microcalcifications.

Some important factors to consider in digital mammography are radiation dosage and image quality. It is important to minimize the patient exposure to radiation. However, low radiation dosage can lead to low signal-to-noise ratios (SNR), which affects image quality. To improve SNR, larger detector pixel dimensions can be used but at the expense of image resolution. Fortunately, the image resolution can be enhanced by multiframe registration techniques. In particular, Robinson *et al.* [7] showed that mammographic images with similar quality as a single image acquired at a normal dosage of 226 mAs, can be produced using multiple images at a reduced combined dosage of 169.5 mAs. In this case, a set of spatially shifted low radiation images are acquired, and a higher resolution image is composed representing the registered image set. In practice, the image shifts can be obtained by X-ray tube rotations, or by moving the imaged object with respect to the X-ray source. Also, in some cases, the shifted images are acquired by a set of sensors spatially displaced [8]. The key advantage to this approach is that high-resolution mammographic images can be obtained by combining lower radiation images. As such, multisource superresolution reconstruction is a promising algorithmic solution for obtaining mammographic images with resolutions higher than can be achieved by the physical radiographic hardware in a single image at a given dosage, thereby improving the visibility of suspicious structures. Multisource superresolution reconstruction techniques also can help avoiding patient discomfort, and additional X-ray exposure, when suspicious breast structures are re-examined in higher detail, providing higher quality image scaling than other available methods, as discussed later in this correspondence.

Given the benefits of image superresolution, several methods have been proposed for the purpose of enhancing medical images. Greenspan *et al.* [1] and Kennedy *et al.* [2], [3] utilized the iterative back-projection (IBP) method proposed by Irani *et al.* [4] to construct high-resolution magnetic resonance (MR) and positron emission tomography (PET) images, respectively, from spatially shifted images. In the IBP approach, an estimate of the high-resolution image is compare with low-resolution image estimates. The differences between the estimated low-resolution images and the actual low-resolution images are then used to refine the high-resolution image in an iterative manner. Hsu *et al.* [5] proposed to create high-resolution cardiovascular images using a superresolution method based on projection on convex sets (POCS) [6]. In the POCS approach, a convex constraint set is set up to maintain consistency with the low-resolution images. The estimated high-resolution image is projected onto each constraint within the convex constraint set until the desired condition is satisfied. Other super-resolution methods include maximum *a posteriori* methods [7], [9], Bayesian methods [10], neural network methods [11], and wavelet-based methods [12]. One major drawback to existing methods is that they treat all image content equally from a structural perspective. This leaves enhancing the visual fidelity of the high-resolution medical images based on the structural characteristics of the underlying image content largely unexplored. This is particularly important in enhancing mammographic images, where the structural detail of the breast region being imaged is critical to the early clinical diagnosis of cancer, improving the chances of success of breast cancer treatments.

The main contribution of this paper is a novel superresolution method for producing high-resolution mammographic images. The proposed method is based on complex wavelet phase information and tunes the high-resolution image for improved detail visibility. In this paper, the superresolution problem is described in the context of mammographic images in Section II. The proposed method is described in Section III. Experimental results are presented and discussed in Section IV. Finally, conclusions are drawn in Section V.

II. Problem Formulation

The multisource image superresolution problem can be formulated in the context of mammographic images as follows. Consider n 2-D low-resolution mammographic images $f_1, f_2, \ldots, f_n$ of size $M \times N$. Each low-resolution image can be viewed as being acquired from a single high-resolution source image g of size $RM \times RN$ (where R is the resolution enhancement factor), under various forms of signal degradation such as decreased sampling, warping, and blurring. Low-resolution images can undergo different degradations, and a low-resolution image f_i is represented in the following matrix-vector form:

$$(\underline{f}_i)_{:} = \mathrm{H_i}(\underline{g})_{:} + \underline{n}_i \tag{1}$$

where $(\underline{f}_i)_{:}$ is a $[MN \times 1]$ vector representing a low-resolution image f_i lexicographically ordered, $(\underline{g})_{:}$ is a $[R^2MN \times 1]$ vector representing the high-resolution image g lexicographically ordered, $\mathrm{H_i}$ is a $[MN \times R^2MN]$ matrix representing the degradation function for a low-resolution image, and $\underline{n}_i$ is a $[MN \times 1]$ noise vector added to a low-resolution image. The degradation function typically is composed of multiple degradation functions, modeling different types of image degradation and can be derived based on the characteristics of the imaging device.

The relationship between all n low-resolution images and the high-resolution image can then be expressed as follows:

$$\begin{bmatrix} (\underline{f}_1)_{:} \\ (\underline{f}_2)_{:} \\ \vdots \\ (\underline{f}_n)_{:} \end{bmatrix} = \begin{bmatrix} \mathrm{H_1} \\ \mathrm{H_2} \\ \vdots \\ \mathrm{H_n} \end{bmatrix} (\underline{g})_{:} + \begin{bmatrix} \underline{n}_1 \\ \underline{n}_2 \\ \vdots \\ \underline{n}_n \end{bmatrix}. \tag{2}$$

For the sake of simplicity, (2) can be expressed in the following form:

$$\overline{\underline{f}} = \overline{\mathrm{H}}(\underline{g})_{:} + \overline{\underline{n}} \tag{3}$$

where $\overline{\underline{f}}$ indicates a vector composed of vectors $\underline{f}_1, \underline{f}_2, \ldots, \underline{f}_n$ stacked on top of each other, and $\overline{\mathrm{H}}$ indicates a matrix composed of matrices $\mathrm{H_1}, \mathrm{H_2}, \ldots, \mathrm{H_n}$ stacked on top of each other. Using the above relationship between the low-resolution image and the source high-resolution image, the multisource image superresolution problem can be formulated as an inverse problem, where a model of the high-resolution source image g is derived from the observed low-resolution images $f_1, f_2, \ldots, f_n$. This multisource image superresolution problem is underdetermined, and no unique solution exists.

III. Proposed Method

The proposed method can be briefly described as follows. First, complex wavelet phase information is extracted from the low-resolution mammographic images. Second, the superresolution problem is formulated as a constrained optimization problem, using a third-order Markov prior model that is adapted based on phase coherence moments derived from the complex wavelet phase information. This optimization problem can then be solved using an iterative solver.

A. Complex Wavelet Phase Information Extraction

The proposed method has been designed to reconstruct high-resolution mammographic images, while preserving structural details of these images so that a better visualization of the patient conditions can be achieved. Therefore, it is necessary to use a method for measuring the structural significance of breast features in the individual low-resolution images, so more of the relevant details are better preserved in the image reconstruction. A recent approach that has been shown to be particularly effective in measuring structural significance of image characteristics is the use of complex wavelet phase information [13]–[17].

A particularly important complex wavelet phase characteristic with respect to structural significance is phase coherence. Such techniques are based on the postulate that structurally significant signal characteristics occur at points in a signal, where there is maximal phase order in a frequency domain representation of the signal. Furthermore, local phase coherence is insensitive to local contrast and intensity variations in an image, which can be important in the case of mammographic images. Considering these benefits, local phase coherence is utilized by the proposed method to measure the significance of features in a mammographic image.

In the proposed method, complex-valued Log–Gabor wavelets [18] are used to obtain localized frequency information from a low-resolution mammographic image at different scales c and orientations θ. Given an image I, the local amplitude A and phase ϕ at a particular scale c and orientation θ can be determined as follows:

$$A_c(\underline{x},\theta) = \sqrt{\left(I(\underline{x}) * F_c^e(\theta)\right)^2 + \left(I(\underline{x}) * F_c^o(\theta)\right)^2} \tag{4}$$

$$\phi_c(\underline{x},\theta) = \tan^{-1}\left(\frac{\left(I(\underline{x}) * F_c^e(\theta)\right)}{\left(I(\underline{x}) * F_c^o(\theta)\right)}\right) \tag{5}$$

where $F_c^e(\theta)$ and $F_c^o(\theta)$ are the pair of even-symmetric and odd-symmetric Log–Gabor wavelets at scale c and orientation θ, and $\underline{x}$ denotes the image point (x, y). Given amplitude A and phase ϕ, a measure of local phase coherence at a particular orientation θ was proposed by Morrone *et al.* [13] as the amplitude-weighted sum of local phase deviations $\Delta\Phi_c(\underline{x},\theta)$ across multiple scales relative to the mean phase $\bar{\phi}(\underline{x},\theta)$ across multiple scales

$$P(\underline{x},\theta) = \frac{\sum_c A_c(\underline{x},\theta)\Delta\Phi_c(\underline{x},\theta)}{\sum_c A_c(\underline{x},\theta)} \tag{6}$$

where

$$\Delta\Phi_c(\underline{x},\theta) = \cos\left(\phi_c(\underline{x},\theta) - \bar{\phi}(\underline{x},\theta)\right). \tag{7}$$

From (6), it can be observed that as the individual wavelet components approach maximal phase order, representing maximal structural significance, the local phase deviation terms $\Delta\Phi_c(\underline{x},\theta)$ approach one across scales, the amplitude-weighted sum of local phase deviations approaches the sum of individual amplitudes and the local phase coherence measure $P(\underline{x},\theta)$ approaches one. As the wavelet components become maximally out of phase, representing minimal structural significance, the local phase deviation terms $\Delta\Phi_c(\underline{x},\theta)$ approach zero and the local phase coherence measure $P(\underline{x},\theta)$ approaches zero. The main advantage of the aforementioned measure is that it depends primarily on phase information, thereby largely invariant to the local contrast and intensity variations found in mammographic images.

Two important issues with the formulation of local phase coherence proposed by Morrone *et al.* [13] is that it is sensitive to noise and provides poor structural feature sensitivity and localization [15]. To address these issues, the proposed method utilizes a modified measure of local phase coherence proposed by Kovesi [15], which improves phase coherence sensitivity as well as reduces noise sensitivity. To improve phase coherence sensitivity, it was proposed that the phase deviation term $\Delta\Phi_c(\underline{x},\theta)$ can instead be formulated based on the fact that when maximal phase order occurs, the cosine of the phase deviation is large, and the absolute value of the sine of the phase deviation is small

$$\Delta\Phi_c(\underline{x},\theta) = \cos\left(\phi_c(\underline{x},\theta) - \bar{\phi}(\underline{x},\theta)\right) - \left|\sin\left(\phi_c(\underline{x},\theta) - \bar{\phi}(\underline{x},\theta)\right)\right|. \tag{8}$$

To further improve phase coherence localization, it was proposed that a phase coherence weighting function W be introduced across wider frequency spreads. The higher W, the higher the phase coherence across wider frequency spreads, and the greater is the local structural significance [15]. To reduce noise sensitivity, it was proposed by Kovesi [16] that a noise threshold T be applied to the product of the amplitude A_c and the phase deviation term $\Delta\Phi_c(\underline{x},\theta)$, for each scale c, to reduce the effect of noise prior to normalization by the sum of individual amplitudes

$$P(\underline{x},\theta) = \frac{\sum_c W(\underline{x},\theta)\left\lfloor A_c(\underline{x},\theta)\Delta\Phi_c(\underline{x},\theta) - T\right\rfloor}{\sum_c A_c(\underline{x},\theta) + \varepsilon} \tag{9}$$

where ε is a small constant to prevent division by zero. The values of W, c, and T used during testing are the same as those outlined in [16].

Since we wish to obtain a single measure of structural significance for low-resolution mammographic image features, it is necessary to combine the local phase coherence information, computed for the different wavelet orientations, in such a way that takes advantage of the variations in local phase coherence due to orientation. In the proposed method, a moment analysis approach was used to combine local phase coherence information. This approach is based on that proposed by Kovesi *et al.* [16], as it was shown to provide improved structural feature localization over existing methods. The second-order moments of phase coherence are computed to determine a phase coherence covariance matrix Λ in each image point $\underline{x}$ [see (10) shown at the bottom of the page].

The eigenvalues of $\Lambda(\underline{x})$ can then be obtained by eigendecomposition, and corresponds to the squared length of the major and minor axes of local phase coherence. The maximum complex wavelet phase coherence moment $\mu(\underline{x})$ corresponds to the largest eigenvalue of $\Lambda(\underline{x})$ and was shown to be a good indication of structural significance [16]. Given that $\Lambda(\underline{x})$ is a 2×2 matrix, the maximum moment $\mu(\underline{x})$ can be expressed as shown in (11) at the bottom of the next page.

A high value of $\mu(\underline{x})$ implies strong structural significance of the local feature at $\underline{x}$, in the low-resolution mammographic image, and should be well preserved in the reconstructed high-resolution mammographic image.

B. Constrained Optimization With Phase-Adaptive Prior Model

With the phase-based measure of structural significance of mammographic image features in place, it is necessary to determine how this information can be used to enhance the visual fidelity of the high-resolution mammographic image. The superresolution problem posed in (3), can be formulated as an optimization problem as follows:

$$(\underline{\hat{g}})_{:} = \arg\min\left(\left\|\overline{\mathrm{H}}(\underline{g})_{:} - \underline{\bar{f}}\right\|\right) \tag{12}$$

$$\Lambda(\underline{x}) = \begin{bmatrix} \sum_\theta \left(P(\underline{x},\theta)\cos(\theta)\right)^2 & \sum_\theta \left(P(\underline{x},\theta)\sin(\theta)\right)\left(P(\underline{x},\theta)\cos(\theta)\right) \\ \sum_\theta \left(P(\underline{x},\theta)\sin(\theta)\right)\left(P(\underline{x},\theta)\cos(\theta)\right) & \sum_\theta \left(P(\underline{x},\theta)\sin(\theta)\right)^2 \end{bmatrix} \tag{10}$$

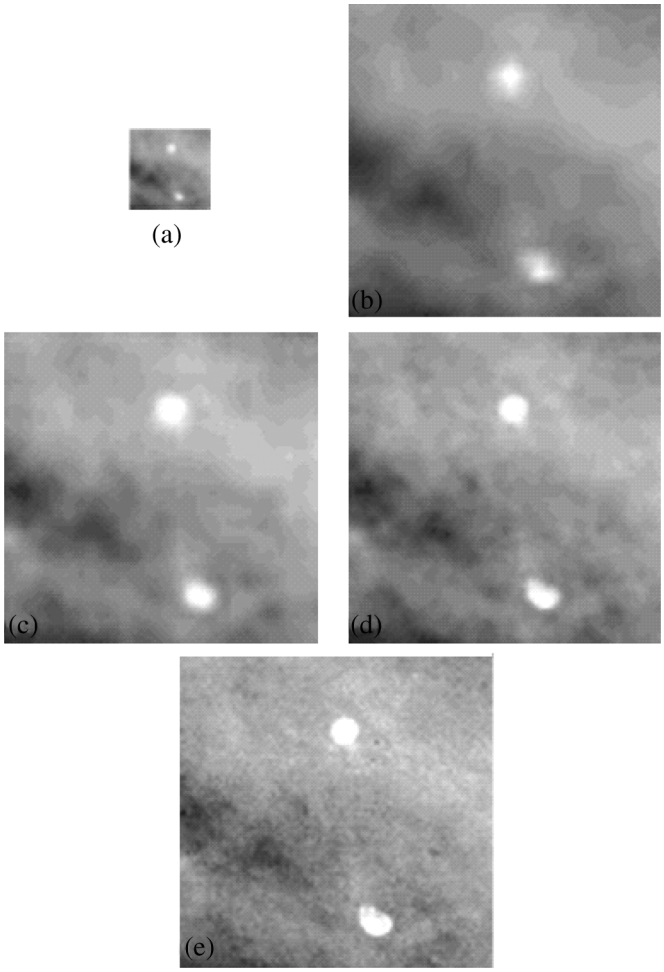

Fig. 1. ROI from TEST 1: a) low-resolution image, b) bicubic interpolation, c) IBP method, d) proposed method, and e) reference image.

TABLE I
PSNR FOR TEST DATA-SETS

Image	PSNR (dB)		
	Bicubic Interpolation	IBP Method	Proposed Method
TEST 1	25.94	29.78	32.39
TEST 2	21.54	27.01	29.66
TEST 3	20.83	28.52	31.17
TEST 4	28.86	32.55	34.85
TEST 5	29.53	31.71	34.48

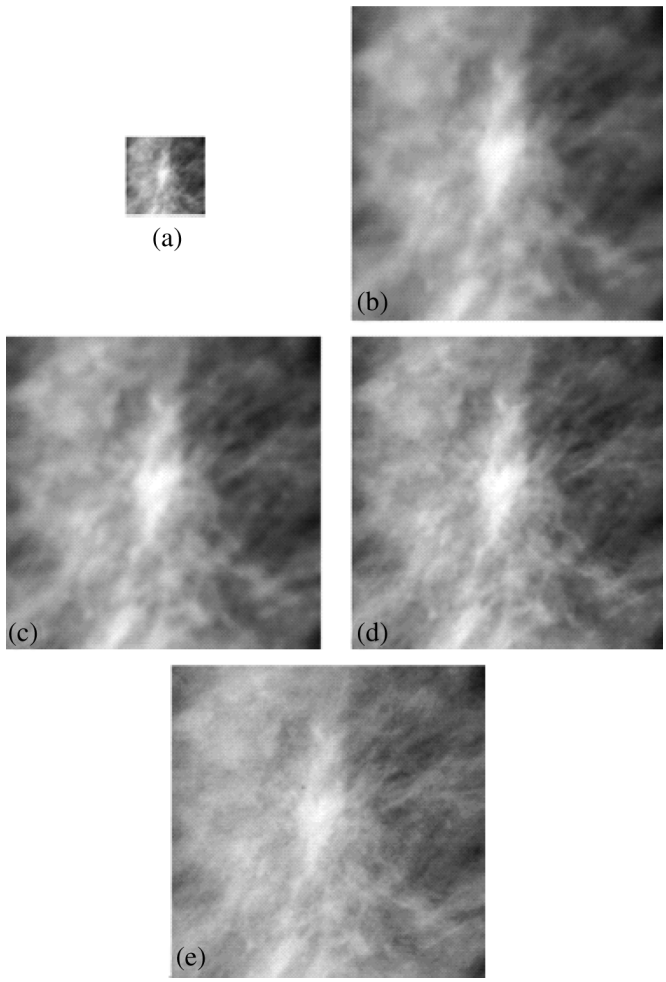

Fig. 2. ROI from TEST 2: a) low-resolution image, b) bicubic interpolation, c) IBPmethod, d) proposed method, and e) reference image.

where $(\hat{\underline{g}})_{:}$ is a vector representing the estimated high-resolution image $\hat{g}$ lexicographically ordered.

In real-world situations, we often have only a few mammographic image acquisitions made to limit patient discomfort and radiation exposure. Therefore, the problem described in (12) is under-determined and, therefore, ill-posed. One method of regularizing this ill-posed problem is to impose a prior model onto the system, such that a unique solution can be found. This regularized superresolution problem can be expressed as follows:

$$(\hat{\underline{g}})_{:} = \arg\min\left(\left\|\overline{\mathrm{H}}(\underline{g})_{:} - \bar{\underline{f}}\right\| + \left\|\Gamma(\underline{g})_{:}\right\|\right) \tag{13}$$

where Γ represents the prior constraints. Given this formulation, we wish to impose a set of prior constraints on the superresolution problem that provides a smooth, unbiased estimation of the high-resolution mammographic image, using the low-resolution mammographic images without unexpected variations. Using a third-order Markov model [19], the proposed method imposes second-order thin plate

$$\mu(\underline{x}) = \frac{1}{2}\left(\sum_{\theta}\left[\left(P(\underline{x},\theta)\sin(\theta)\right)^2 + \left(P(\underline{x},\theta)\cos(\theta)\right)^2\right] + \sqrt{4\left(\sum_{\theta}\left(P(\underline{x},\theta)\sin(\theta)\right)\left(P(\underline{x},\theta)\cos(\theta)\right)\right)^2 + \left(\sum_{\theta}\left[\left(P(\underline{x},\theta)\cos(\theta)\right)^2 - \left(P(\underline{x},\theta)\sin(\theta)\right)^2\right]\right)^2}\right) \tag{11}$$

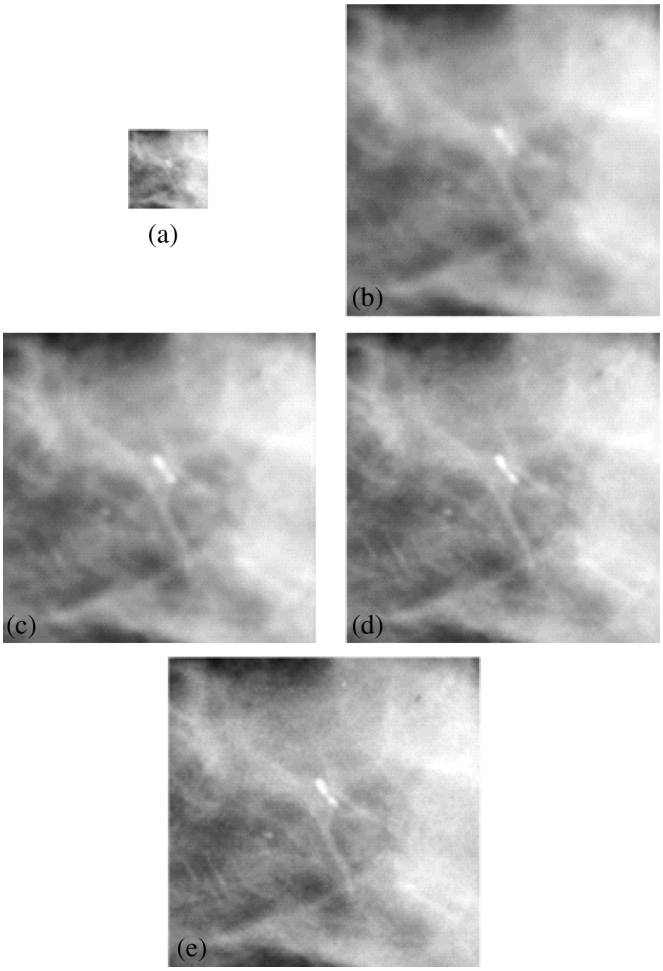

Fig. 3. ROI from TEST 3: a) low-resolution image, b) bicubic interpolation, c) IBP method, d) proposed method, e) reference image.

spline [20] constraints on each point $\underline{x} = (x, y)$, which minimizes an approximate curvature and can be expressed as follows:

$$\|\Gamma(g)\| = \int\int \left[\left(\frac{\partial^2 g}{\partial^2 x} \right)^2 + 2 \left(\frac{\partial^2 g}{\partial x \partial y} \right)^2 + \left(\frac{\partial^2 g}{\partial^2 y} \right)^2 \right] dx dy. \tag{14}$$

Based on the aforementioned third-order Markov prior constraints and discrete approximations of partial derivatives, the prior constraints term Γ can be expressed for each point $\underline{x}$ in matrix form, as follows:

$$\Gamma(\underline{x}) = \begin{bmatrix} 0 & 0 & 1 & 0 & 0 \\ 0 & 2 & -8 & 2 & 0 \\ 1 & -8 & 20 & -8 & 1 \\ 0 & 2 & -8 & 2 & 0 \\ 0 & 0 & 1 & 0 & 0 \end{bmatrix}. \tag{15}$$

The central element of the matrix $\Gamma(\underline{x})$ represents $\underline{x}$. One effective approach to enhancing the visual fidelity of the high-resolution mammographic image is to adapt the prior constraints based on phase coherence characteristics, preserving important structural characteristics of the breast tissues.

In the proposed method, the third-order Markov prior constraints imposed at each mammographic image location are adaptively scaled, based on phase coherence characteristics. This form of scaling allows fine-grained control over the level of approximation at each point in the image. As the scaling increases, system conditioning is improved, while the level of approximation is reduced. As such, the scaling of prior constraints can be adjusted to either preserve image characteristics by using smaller scalars, or provide a smoother estimate of image characteristics by using larger scalars. In clinical diagnosis of breast cancer, we are motivated to reduce scaling to avoid over-smoothing at image points with high phase coherence. At the same time, it is important to suppress image degradation and noise in areas of low phase coherence, avoiding misdiagnosis due to imaging anomalies. As such, we are motivated to increase scaling to provide a smoother approximation, and reduce such degradation and noise.

The aforementioned conflicting motivations are accommodated as follows. At each point of the mammographic image $\underline{x}$, the scalar applied to the third-order Markov prior constraints is determined using a square root scaling function, which is based on the maximum complex wavelet phase coherence moments

$$\alpha(\underline{x}) = \sqrt{\alpha_{\min} + (1 - \mu(\underline{x}))(\alpha_{\max} - \alpha_{\min})} \tag{16}$$

where $\alpha_{\max}$ and $\alpha_{\min}$ are the maximum and minimum scalars, and $\mu(\underline{x})$ is the maximum phase coherence moment. It can be observed from (16) that as the maximum phase coherence moment increases, the scalar α decreases. This formulation agrees with our motivations as mammographic features with high structural significance (indicated by high phase coherence moments) are preserved (by reducing scaling), and mammographic features with weak structural significance (indicated by low phase coherence moments) are smoothed (by increasing scaling) to reduce degradation and noise. The square root term in (16) is designed to decrease the rate of influence of lower magnitudes of maximum phase coherence moments (representing mammographic features with weak structural significance), and increase the rate of influence of higher magnitudes of phase coherence moments (representing mammographic features with high structural significance). For testing purposes, $\alpha_{\max}$ and $\alpha_{\min}$ are set to 1.0 and 0.3, respectively.

What this accomplishes is to adaptively adjust the contribution of information from the low-resolution mammographic images to the reconstruction of the high-resolution mammographic image. In this way, important structural characteristics of breast tissues are emphasized for improved visualization. The maximum phase coherence moment used is extracted from the low-resolution mammographic images used in the reconstruction process, averaged, and up-sampled to the same resolution as the estimated high-resolution mammographic image. The prior constraints associated with each image location is then multiplied by the calculated scalar $\alpha(\underline{x})$. The final moment-adaptive prior constraints Γ can be defined based on the following expression:

$$\|\Gamma(g)\| = \int\int \alpha(x, y) \times \left[\left(\frac{\partial^2 g}{\partial^2 x} \right)^2 + 2 \left(\frac{\partial^2 g}{\partial x \partial y} \right)^2 + \left(\frac{\partial^2 g}{\partial^2 y} \right)^2 \right] dx dy \tag{17}$$

or in matrix form

$$\Gamma(\underline{x}) = \begin{bmatrix} 0 & 0 & \alpha(\underline{x}) & 0 & 0 \\ 0 & 2\alpha(\underline{x}) & -8\alpha(\underline{x}) & 2\alpha(\underline{x}) & 0 \\ \alpha(\underline{x}) & -8\alpha(\underline{x}) & 20\alpha(\underline{x}) & -8\alpha(\underline{x}) & \alpha(\underline{x}) \\ 0 & 2\alpha(\underline{x}) & -8\alpha(\underline{x}) & 2\alpha(\underline{x}) & 0 \\ 0 & 0 & \alpha(\underline{x}) & 0 & 0 \end{bmatrix}. \tag{18}$$

The high-resolution mammographic image is obtained by solving a phase-adaptive constrained optimization problem, using an iterative solver such as the LSQR algorithm [21].

IV. Experimental Results

To illustrate the effectiveness of the proposed resolution enhancement method in terms of visual fidelity, the proposed method was tested using digital mammographic images obtained from the Mammographic

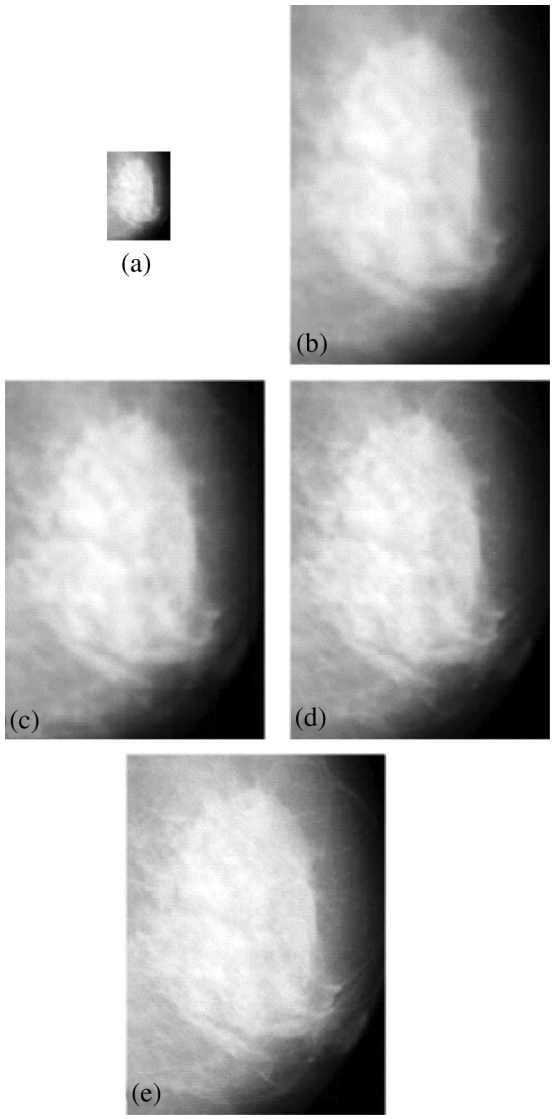

Fig. 4. ROI from TEST 5: a) low-resolution image, b) bicubic interpolation, c) IBP method, d) proposed method, and e) reference image.

Image Analysis Society (MIAS) database [23]. The system used to acquire the mammographic images was a Joyce–Loebl microdensitometer SCANDIG-3, with a linear response in the optical density range 0–3.2. Each mammographic image is 8-bit grayscale with a pixel resolution of $50\ \mu$m $\times\ 50\ \mu$m. The test data-sets can be summarized as follows.

1) **TEST 1**: MIA database mammogram 002. Background tissue: fatty-glandular. Class of abnormality: well-defined/circumscribed masses. Severity of abnormality: benign.
2) **TEST 2**: MIA database mammogram 145. Background tissue: dense-glandular. Class of abnormality: spiculated masses. Severity of abnormality: benign.
3) **TEST 3**: MIA database mammogram 148. Background tissue: fatty. Class of abnormality: spiculated masses. Severity of abnormality: malignant.
4) **TEST 4**: MIA database mammogram 211. Background tissue: fatty-glandular. Class of abnormality: calcification. Severity of abnormality: malignant.
5) **TEST 5**: MIA database mammogram 212. Background tissue: fatty-glandular. Class of abnormality: calcification. Severity of abnormality: benign.

Each data-set consists of six low-resolution mammographic images generated from a reference mammographic image. To simulate low-resolution and low dosage conditions, each low-resolution mammographic image is generated by applying a 4×4 average blur, Poisson-distributed noise (to simulate quantum noise in mammographic images [22]), a spatial shift (based on the arbitrarily chosen translations $(\Delta x, \Delta y) = \{(0,0),\ (0.5,0),\ (0.25,0.25),\ (0,0.5),(0.75,0.5),\ (0.5,0.75)\}$), as well as a resolution reduction by a factor of 4 with respect to the reference mammographic image. The underlying goal is to increase the resolution by a factor of 4 in each dimension. For comparison purposes, Bicubic interpolation and the iterative back-projection (IBP) method [4] were evaluated. The IBP method was tested since it has been used by Greenspan *et al.* [1] and Kennedy *et al.* [2], [3] for medical image superresolution purposes. To evaluate the performance of the proposed method in a quantitative manner, the peak-signal-to-noise ratio (PSNR) was computed for the resolution enhanced images obtained with the tested algorithms, relative to the reference image used to generate the low-resolution images.

The PSNR results for all the test data-sets are summarized in Table I. It can be observed that the PSNR values for the mammographic images generated using the proposed method are noticeably higher than those produced using the other methods, for all test data-sets. To visualize the improvements obtained from using the proposed method, regions of interest (ROI) extracted from the high-resolution mammographic images produced using the evaluated methods for TEST 1, TEST 2, TEST 3, and TEST 5 are shown in Figs. 1–4, respectively. It is important to note the images were contrast enhanced through intensity normalization to improve visibility of details in the figures. It can be seen that the proposed method produces high-resolution mammographic images with noticeably improved visual fidelity compared to other methods, both quantitatively and visually. In TEST 1, the shape and boundaries of the calcifications are better defined in the superresolution image obtained with the proposed method. In TEST 2, the nodule boundaries are difficult to interpret in the high-resolution mammographic image obtained using bicubic interpolation. Both IBP and the proposed method provide noticeably improved structural detail pertaining to the nodule boundary, with the proposed method providing improved structural contrast around the boundary when compared to the IBP method. In TEST 3, there is a calcification behind dense tissues that is very difficult to interpret in the high-resolution mammographic image obtained using bicubic interpolation. Both IBP and the proposed method provide noticeably improved structural detail pertaining to the calcification, with the proposed method providing improved structural contrast over the IBP method. It can be seen in TEST 5 that both IBP and the proposed method provide sharper images of the masses compared with bicubic interpolation. However, the shape, boundaries and structure of the masses tend to be better defined in the image provided by the proposed method.

V. Conclusion

In this paper, we introduced a novel phase-adaptive superresolution approach, designed to facilitate detailed visual screening of mammographic images. The reconstructed high-resolution mammographic image can be tuned to preserve and accentuate important structural characteristics of breast tissues, improving the visibility of suspicious structures, such as nodule boundaries and calcifications. The proposed method solves the multisource image superresolution reconstruction problem using complex wavelet phase information, and imposing third-order Markov prior constraints. Experimental results are illustrated using mammographic images from the Mammographic Image Analysis Society (MIAS) database [23], and we show that improved visual fidelity can be achieved using the proposed

method when compared to existing techniques. Future work involve the integration of intensity remapping techniques into the proposed superresolution method to correct for signal nonhomogeneities in the acquired mammographic images. Also, we plan on integrating contrast enhancement to further accentuate structural characteristics in breast tissues. Furthermore, we plan on evaluating the proposed method for other types of imaging modalities such as MR and PET against more superresolution methods.

ACKNOWLEDGMENT

The authors would like to thank the Mammographic Image Analysis Society for the mammographic images used during testing.

REFERENCES

[1] H. Greenspan, G. Oz, N. Kiryati, and S. Peled, "Super-resolution in MRI," in *Proc. IEEE Int. Symp. Biomedical Imaging*, 2002, pp. 943–946.

[2] J. Kennedy, O. Israel, A. Frenkel, R. Bar-Shalom, and H. Azhari, "Super-resolution in PET imaging," *IEEE Trans. Med. Imag.*, vol. 25, no. 2, pp. 137–147, Feb. 2006.

[3] J. Kennedy, O. Israel, A. Frenkel, R. Bar-Shalom, and H. Azhari, "Improved image fusion in PET/CT using hybrid image reconstruction and super-resolution," *Int. J. Biomed. Imag.*, vol. 2007, 2007, Article ID 46846, 10 pp..

[4] M. Irani and S. Peleg, "Improving resolution by image registration," in *Proc. CVGIP: Graph. Model. Image Process.*, 1991, vol. 53, no. 3, pp. 231–239.

[5] J. Hsu, C. Yen, C. Li, M. Sun, B. Tian, and M. Kaygusuz, "Application of wavelet-based POCS super-resolution for cardiovascular MRI image enhancement," in *Proc. Int. Conf. Image Graph.*, 2004, pp. 572–575.

[6] K. Sauer and J. Allebach, "Iterative reconstruction of band-limited images from nonuniformly spaced samples," *IEEE Trans. Circuits Syst.*, vol. 34, no. 12, pp. 1497–1506, Dec. 1987.

[7] D. Robinson, S. Farsiu, J. Lo, P. Milanfar, and C. Toth, "Efficient multiframe registration of aliased X-ray images," presented at the 41st Asilomar Conf. Signals, Systems, and Computers, 2007.

[8] T. Aoki, Y. Ishida, H. Morii, Y. Tomita, G. Ohashi, J. Temmyo, and Y. Hatanaka, "Super-resolution X-ray imaging by CdTe discrete detector arrays," presented at the SPIE—Hard X-Ray and Gamma-Ray Detector Physics VII, 2005.

[9] A. Lettington and Q. Hong, "Ringing artifact reduction for Poisson MAP superresolution algorithms," *IEEE Signal Process. Lett.*, vol. 2, no. 5, pp. 83–84, May 1995.

[10] A. Kanemura, S. Maeda, and S. Ishii, "Hyperparameter estimation in bayesian image superresolution with a compound Markov random field prior," in *Proc. IEEE Workshop on Machine Learning for Signal Processing*, 2007, pp. 181–186.

[11] M. Nguyen, P. Atkinson, and H. Lewis, "Superresolution mapping using a Hopfield neural network with lidar data," *IEEE Geosci. Remote Sens. Lett.*, vol. 2, no. 3, pp. 366–370, Mar. 2005.

[12] N. Nguyen and P. Milanfer, "An efficient wavelet-based algorithm for image super resolution," in *Proc. Int. Conf. Image Process.*, 2000, vol. 2, pp. 351–354.

[13] M. Morrone and R. Owens, "Feature detection from local energy," *Pattern Recognit. Lett.*, vol. 6, pp. 303–313, 1987.

[14] M. Morrone and D. Burr, "Feature detection in human vision: A phase-dependent energy model," *Proc. Roy. Soc. London B*, vol. 235, pp. 221–245, 1988.

[15] P. Kovesi, "Phase congruency: A low-level image invariant," *Psych. Res.*, vol. 64, no. 2, pp. 136–148, 2000.

[16] P. Kovesi, "Phase congruency detects corners and edges," in *Proc. Australian Pattern Recognition Soc. Conf.*, 2003, pp. 309–318.

[17] Z. Wang and E. Simoncelli, "Local phase coherence and the perception of blur," *Advances in Neural Information Processing Systems*, vol. 16, May 2004.

[18] D. Field, "Relations between the statistics of natural images and the response properties of cortical cells," *J. Opt. Soc. Amer. A*, vol. 4, no. 12, pp. 2379–2394, 1987.

[19] A. Rangarajan and R. Chellappa, "Markov random field models in image processing," in *Handbook of Brain Theory and Neural Networks*. Cambridge, MA: MIT Press, 1998, pp. 564–567.

[20] G. Wahba, *Spline Models for Observational Data*. Philadelphia, PA: SIAM, 1990.

[21] C. Paige and M. Saunders, "LSQR: An algorithm for sparse linear equations and sparse least squares," *ACM Trans. Math. Softw.*, vol. 8, no. 1, pp. 43–71, 1982.

[22] G. Barnes and D. Chakraborty, "Radiographic mottle and patient exposure in mammography," *Radiology*, vol. 145, pp. 815–821, 1982.

[23] J. Suckling, J. Parker, D. Dance, S. Astley, I. Hutt, C. Boggis, I. Ricketts, E. Stamatakis, N. Cerneaz, S. Kok, P. Taylor, D. Betal, and J. Savage, "The mammographic images analysis society digital mammogram database," *Exerpta Medica. Int. Congr. Ser.*, vol. 1069, pp. 375–378, 1994.